



Cite this: *Phys. Chem. Chem. Phys.*,  
2023, 25, 23829

# On the impact of adsorbed gas molecules on the anisotropic electro-optical properties of $\beta_{12}$ -borophene

Nguyen N. Hieu,<sup>a</sup> Chuong V. Nguyen,<sup>c</sup> Huynh V. Phuc<sup>d</sup> and Bui D. Hoi<sup>b,\*e</sup>

We theoretically study the role of adsorbed gas molecules on the electronic and optical properties of monolayer  $\beta_{12}$ -borophene with {a,b,c,d,e} atoms in its unit cell. We focus our attention on molecules  $\text{NH}_3$ ,  $\text{NO}$ ,  $\text{NO}_2$ , and  $\text{CO}$ , which provide additional states permitted by the host electrons. Utilizing the six-band tight-binding model based on an inversion symmetry (between {a,e} and {b,d} atoms) and the Kubo formalism, we survey the anisotropic electronic dispersion and the optical multi-interband spectrum produced by molecule-boron coupling. We consider the highest possibilities for the position of molecules on the boron atoms. For molecules on {a,e} atoms, the inherent metallic phase of  $\beta_{12}$ -borophene becomes electron-doped semiconducting, while for molecules on {b,d} and c atoms, the metallic phase remains unchanged. For molecules on {a,e} and {b,d} atoms, we observe a redshift (blueshift) optical spectrum for longitudinal/transverse (Hall) component, while for molecules on c atoms, we find a redshift (blueshift) optical spectrum for longitudinal (transverse/Hall) component. We expect that this study provides useful information for engineering field-effect transistor-based gas sensors.

Received 27th April 2023,  
Accepted 21st August 2023

DOI: 10.1039/d3cp01938a

rsc.li/pccp

## 1 Introduction

Since 2004–2005, starting from graphene,<sup>1,2</sup> two-dimensional (2D) structures have been the best active systems in the industry. However, the electronic devices based on graphene are limited due to its linear dispersion energy, which makes its fermions massless (gapless phase). To overcome this issue, other 2D systems have been searched. For instance, electrons in silicene,<sup>3,4</sup> germanene,<sup>5</sup> stanene,<sup>6</sup> and molybdenum disulfide<sup>7</sup> with an intrinsic spin–orbit coupling are massive (for gap opening). Additionally, the inherent anisotropy feature of phosphorene<sup>8,9</sup> has highlighted it as a material with a high on–off current ratio and high mobility for charge carriers in field-effect transistors.<sup>10,11</sup>

Borophene, a single-layer of boron atoms (located at the boundary between metals and non-metals), is also a known 2D material with various metallic phases.<sup>12–20</sup> Metallic phases differ depending on the configuration of boron atoms in the

layer. While the most studied configurations are striped,  $\beta_{12}$ ,  $\chi_3$ , and honeycomb,  $\beta_{12}$ -borophene is known to be the most stable allotrope.<sup>21,22</sup>

Numerous applications have been found for 2D-based logic devices such as diodes, transistors, capacitors, memories, and highly sensitive sensors.<sup>23–25</sup> Particularly, it has been well understood that faster response and recovery time can be found in graphene-based sensors compared to common traditional sensors.<sup>26–28</sup> For instance, O. Leenaerts *et al.*<sup>29</sup> have investigated the adsorption of  $\text{H}_2\text{O}$ ,  $\text{NH}_3$ ,  $\text{CO}$ ,  $\text{NO}_2$ , and  $\text{NO}$  on a graphene substrate using first-principles calculations and have demonstrated the sensitivity of the graphene-based gas sensor toward  $\text{H}_2\text{O}$ ,  $\text{CO}$ , and  $\text{NH}_3$  gases is 1 ppb (parts per 10<sup>9</sup>). These, in turn, has led to variation in other electrical properties of the sensor.<sup>30,31</sup>

In the case of borophene, it has been shown that the borophene-based circuits are suitable for gas sensing applications since they are active to hazardous gases.<sup>32–34</sup> For four gas molecules  $\text{NH}_3$ ,  $\text{NO}$ ,  $\text{NO}_2$ , and  $\text{CO}$ , it has been reported that the adsorption energy is high in borophene. Even though there exist a few works on the adsorption properties of borophene both theoretically and experimentally,<sup>32–35</sup> to the best of our knowledge, the investigation of electronic band structure and optical conductivity of gas sensing in  $\beta_{12}$ -borophene has not been addressed so far. In this paper, we address the electro-optical properties of  $\beta_{12}$ -borophene in the presence of gas

<sup>a</sup> Institute of Research and Development, Duy Tan University, Da Nang, 550000, Vietnam

<sup>b</sup> Faculty of Natural Sciences, Duy Tan University, Da Nang, 550000, Vietnam

<sup>c</sup> Department of Materials Science and Engineering, Le Quy Don Technical University, Ha Noi, 100000, Vietnam

<sup>d</sup> Division of Theoretical Physics, Dong Thap University, Cao Lanh, 870000, Vietnam

<sup>e</sup> Faculty of Physics, University of Education, Hue University, Hue, 530000, Vietnam.  
E-mail: buidinhhoi@hueuni.edu.vn

molecules with the aid of a six-band tight-binding model and the Kubo formula. It should be noted that there are various ways to control the electro-optical features of 2D materials. For instance, a mechanical strain<sup>36,37</sup> or oxidation<sup>38</sup> has been applied to affect the optical and electronic properties of borophene. However, here, we aim at engineering the optical responses through adsorbed gas molecules NH<sub>3</sub>, NO, NO<sub>2</sub>, and CO, which results in novel physical insights compared to other methods.

The rest of the paper is organized as follows. In Section 2, we build the Hamiltonian model of  $\beta_{12}$ -borophene in the absence and presence of gas molecules. In Section 3, we present the Kubo formula for the optical conductivity tensor along all directions. In Section 4, we focus on the numerical results and finally, the paper ends in Section 5.

## 2 Hamiltonian model

To build the beloved Hamiltonian model of  $\beta_{12}$ -borophene, we focus on  $p_z$  orbitals of boron atoms since they form the major contribution in the vicinity of the Fermi level.<sup>39–41</sup> The unit cell of  $\beta_{12}$ -borophene with the lattice constant of  $L_c \simeq 2.926$  Å contains five atoms, namely {a,b,c,d,e}, as shown in the gray rectangle of Fig. 1(a). Hence, the pristine tight-binding Hamiltonian reads

$$\mathcal{H}_0 = \sum_{\ell} \varepsilon_{\ell} c_{\ell}^{\dagger} c_{\ell} + \sum_{\ell k} t_{\ell k} c_{\ell}^{\dagger} c_k + \text{H.c.}, \quad (1)$$

where H.c. means Hermitian conjugate,  $c_{\ell}^{\dagger}$  ( $c_{\ell}$ ) stands for the creation (annihilation) of an electron at site  $\ell$ ,  $\varepsilon_{\ell}$  is the on-site energy of electron, and  $t_{\ell k}$  is the interatomic hopping energy; from the inversion symmetry between boron atoms,<sup>40,42</sup> these parameters are found to be  $\varepsilon_a = \varepsilon_e = +0.196$ ,  $\varepsilon_b = \varepsilon_d = -0.058$ ,  $\varepsilon_c = -0.845$ ,  $t_{ab} = t_{de} = -2.04$ ,  $t_{ac} = t_{ce} = -1.79$ , and  $t_{bc} = t_{cd} = -1.84$ ,  $t_{bd} = -1.91$ , and  $t_{ae} = -2.12$  (all in units of eV). It is necessary to mention that the unusual electronic structure of  $\beta_{12}$ -borophene was found by angle-resolved photoemission spectroscopy and validated by first-principles calculations.<sup>40</sup> These parameters are then obtained by fitting first-principles calculation results to confirm the experiment.

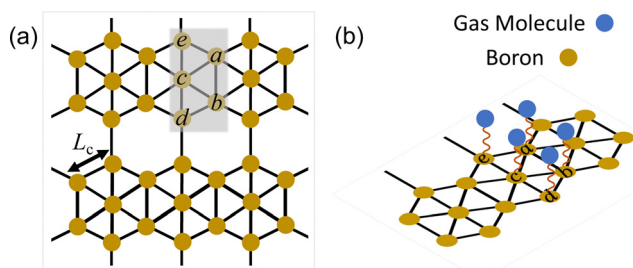


Fig. 1 Geometry structure of  $\beta_{12}$ -borophene including five atoms {a,b,c,d,e} with the lattice constant of  $L_c \approx 2.926$  Å<sup>39–41</sup> (a) without and (b) with adsorbed gas molecules. The shaded area in (a) depicts the rectangular unit cell.

In the absence of gas molecules, using the straightforward Fourier transform, we find the following Hamiltonian in reciprocal-space<sup>39</sup>

$$\mathcal{H}_0(\vec{k}) = \begin{pmatrix} \varepsilon_a & 2t_{ab}g_{\vec{k}} & t_{ac}f_{\vec{k}} & 0 & t_{ae}f_{\vec{k}} \\ 2t_{ab}g_{\vec{k}} & \varepsilon_b & 2t_{bc}g_{\vec{k}} & t_{bd}f_{\vec{k}} & 0 \\ t_{ac}f_{\vec{k}} & 2t_{bc}g_{\vec{k}} & \varepsilon_c & 2t_{cd}g_{\vec{k}} & t_{ce}f_{\vec{k}} \\ 0 & t_{bd}f_{\vec{k}} & 2t_{cd}g_{\vec{k}} & \varepsilon_d & 2t_{de}g_{\vec{k}} \\ t_{ae}f_{\vec{k}} & 0 & t_{ce}f_{\vec{k}} & 2t_{de}g_{\vec{k}} & \varepsilon_e \end{pmatrix}, \quad (2)$$

where  $f_{\vec{k}} = \exp[ik_y L_c / 2\sqrt{3}]$ ,  $g_{\vec{k}} = f_{\vec{k}} \cos(k_x L_c / 2)$ , and  $\vec{k} = (k_x, k_y)$  denotes the electron's momentum.<sup>39,40</sup>

In the presence of gas molecules, we assume that each molecule is adsorbed on one subatom of the borophene each time, e.g., they are adsorbed on all a atoms at the first time. There is another possibility to assume that gas molecules are simultaneously adsorbed on all atoms, but our analysis (not shown here) confirms that this configuration does not provide a significant contribution to the modulation of electronic features compared to the former scenario. In both scenarios, only  $s$  orbital from the gas molecules NH<sub>3</sub>, NO, NO<sub>2</sub>, and CO overlaps with  $p_z$  orbitals of boron atoms. With this, we have a six-band tight-binding Hamiltonian, given by

$$\mathcal{H}(\vec{k}) = \begin{pmatrix} \varepsilon_a & 2t_{ab}g_{\vec{k}} & t_{ac}f_{\vec{k}} & 0 & t_{ae}f_{\vec{k}} & \tilde{t}_a \\ 2t_{ab}g_{\vec{k}} & \varepsilon_b & 2t_{bc}g_{\vec{k}} & t_{bd}f_{\vec{k}} & 0 & \tilde{t}_b \\ t_{ac}f_{\vec{k}} & 2t_{bc}g_{\vec{k}} & \varepsilon_c & 2t_{cd}g_{\vec{k}} & t_{ce}f_{\vec{k}} & \tilde{t}_c \\ 0 & t_{bd}f_{\vec{k}} & 2t_{cd}g_{\vec{k}} & \varepsilon_d & 2t_{de}g_{\vec{k}} & \tilde{t}_d \\ t_{ae}f_{\vec{k}} & 0 & t_{ce}f_{\vec{k}} & 2t_{de}g_{\vec{k}} & \varepsilon_e & \tilde{t}_e \\ \tilde{t}_a & \tilde{t}_b & \tilde{t}_c & \tilde{t}_d & \tilde{t}_e & \tilde{\varepsilon} \end{pmatrix}, \quad (3)$$

where  $\tilde{t}_{\ell}$  and  $\tilde{\varepsilon}$ , respectively, refer to the hopping and on-site energy between the gas molecule and host boron atom. To find  $\tilde{t}_{\ell}$ , we use<sup>43,44</sup>

$$\tilde{t}_{\ell} = \bar{t}_{\ell} \frac{L_c}{d}, \quad (4)$$

where  $d$  is the distance between molecule and borophene sheet and  $\bar{t}_{\ell}$  is the average of other hopping energies on each atom.

For example, for the adsorption on {a,e} atoms, we have  $\bar{t}_{a/e} = \frac{1}{3}(t_{ab} + t_{ac} + t_{ae})$  or on  $c$  atoms, it is  $\bar{t}_c = \frac{1}{4}(t_{ac} + t_{bc} + t_{cd} + t_{ce})$ . On the other hand, for NH<sub>3</sub>, NO, NO<sub>2</sub>, and CO, we respectively have  $d = 1.63, 1.38, 1.57, 1.48$  (all in units of Å). Note that the distance is defined as the center-to-center distance of nearest atoms between the host material and small molecules, i.e. the shortest atom-to-atom distance. This is easily investigated by using density functional computations.<sup>43,44</sup> Also, we respectively set  $\tilde{\varepsilon} = 1.11, 0.95, 1.75, 1.19$  (all in units of eV).<sup>43</sup>

### 3 Optical conductivity

Now, we turn to the Kubo formula<sup>45–47</sup> to calculate the optical conductivity tensor of  $\beta_{12}$ -borophene in the absence and presence of gas molecules. In doing so, we employ the linear response theory, which mainly focuses on the current-current correlation function  $\mathcal{J}_{\alpha\beta}^{\nu\nu'}(\vec{k}) = e^2 \langle \vec{k}, \nu | j_x | \vec{k}, \nu' \rangle \langle \vec{k}, \nu' | j_\beta | \vec{k}, \nu \rangle$ , where  $j_x = \partial \mathcal{H}(\vec{k}) / \partial k_x$  is the current operator and  $\{\alpha, \beta\} = \{x, y\}$  stands for different directions and  $\{\nu, \nu'\}$  refer to different energy bands. Moreover,

$$j_x = -L_c \sin(k_x L_c / 2) \begin{pmatrix} 0 & t_{ab} f_{\vec{k}} & 0 & 0 & 0 & 0 \\ t_{ab} f_{\vec{k}}^* & 0 & t_{bc} f_{\vec{k}} & 0 & 0 & 0 \\ 0 & t_{bc} f_{\vec{k}}^* & 0 & t_{cd} f_{\vec{k}} & 0 & 0 \\ 0 & 0 & t_{cd} f_{\vec{k}}^* & 0 & t_{de} f_{\vec{k}} & 0 \\ 0 & 0 & 0 & t_{de} f_{\vec{k}}^* & 0 & 0 \\ 0 & 0 & 0 & 0 & 0 & 0 \end{pmatrix}, \quad (5a)$$

$$j_y = 2 \cos(k_x L_c / 2) \begin{pmatrix} 0 & t_{ab} \frac{\partial f_{\vec{k}}}{\partial k_y} & \frac{t_{ac}}{2} h_{\vec{k}}^* & 0 & \frac{t_{ac}}{2} h_{\vec{k}} & 0 \\ t_{ab} \frac{\partial f_{\vec{k}}^*}{\partial k_y} & 0 & t_{bc} \frac{\partial f_{\vec{k}}}{\partial k_y} & \frac{t_{bd}}{2} h_{\vec{k}}^* & 0 & 0 \\ \frac{t_{ac}}{2} h_{\vec{k}} & t_{bc} \frac{\partial f_{\vec{k}}^*}{\partial k_y} & 0 & t_{cd} \frac{\partial f_{\vec{k}}}{\partial k_y} & \frac{t_{ce}}{2} h_{\vec{k}}^* & 0 \\ 0 & \frac{t_{bd}}{2} h_{\vec{k}} & t_{cd} \frac{\partial f_{\vec{k}}^*}{\partial k_y} & 0 & t_{de} \frac{\partial f_{\vec{k}}}{\partial k_y} & 0 \\ \frac{t_{ac}}{2} h_{\vec{k}} & 0 & \frac{t_{ce}}{2} h_{\vec{k}}^* & t_{de} \frac{\partial f_{\vec{k}}^*}{\partial k_y} & 0 & 0 \\ 0 & 0 & 0 & 0 & 0 & 0 \end{pmatrix}, \quad (5b)$$

where  $h_{\vec{k}} = \sec(k_x L_c / 2) \frac{\partial f_{\vec{k}}}{\partial k_y}$ .

Next, we use the Kubo formula<sup>48</sup> and the above equations to calculate the optical conductivity tensor:

$$\sigma_{\alpha\beta}(\omega) = i \sum_{\vec{k}} \sum_{\nu, \nu'} \frac{f_{\vec{k}, \nu} - f_{\vec{k}, \nu'}}{\mathcal{E}_{\vec{k}, \nu} - \mathcal{E}_{\vec{k}, \nu'}} \frac{\mathcal{J}_{\alpha\beta}^{\nu\nu'}(\vec{k})}{\hbar\omega + i\delta + \mathcal{E}_{\vec{k}, \nu} - \mathcal{E}_{\vec{k}, \nu'}}, \quad (6)$$

where  $\delta = 50$  meV is a phenomenological factor (it can tune the sharpness of optical peaks) and  $f_{\vec{k}, \nu/\nu'} = 1/[1 + \exp(\mathcal{E}_{\vec{k}, \nu/\nu'}/k_B T)]$  is the Fermi–Dirac distribution function at a temperature of 10 K (the presence of low-energy excitations endows the strongest optical transitions, which requires a small thermal energy  $k_B T$  in  $f_{\vec{k}, \nu/\nu'}$ ).<sup>49</sup> In the above equation, one needs the eigenenergies  $\mathcal{E}_{\vec{k}, \nu}$  and eigenstates  $|\vec{k}, \nu\rangle$  of different bands. However, due to the large size of Hamiltonian, we numerically calculate them. Above equation contains both intraband and interband optical transitions. The intraband transitions at low temperatures mainly

contribute to the optical conductivity in the presence of the disorder or scattering in the THz region due to the role of phonons at low temperatures. This can be described as the Drude-like conductivity, while in a clean system as assumed in the present work, this does not occur. Thus, we focus only on the interband optical transitions. For simplicity, since the imaginary part of conductivity can be easily found *via* the Kramers-Kronig relations,<sup>50</sup> we restrict ourselves only to the real part for optical absorption spectra.

### 4 Numerical results

First, we present the electronic band structure associated with tuning the band gap and electronic phase of  $x$  and  $y$  directions. The calculations are performed *via* a numerical diagonalization of Hamiltonian in eqn (3). Although we provide a general model for all four molecules  $\text{NH}_3$ ,  $\text{NO}$ ,  $\text{NO}_2$ , and  $\text{CO}$ , we only focus on  $\text{NH}_3$  in what follows since other cases only slightly differ quantitatively from the energy scale point of view without qualitatively modifying the results.

The electronic band structures of  $\beta_{12}$ -borophene  $x$  and  $y$  directions are shown in Fig. 2(a) and (e) without the adsorption of molecule  $\text{NH}_3$  inclusion. The inherent metallic phase from the contribution of  $c$  atoms in Fig. 1 in the band is observed in the dotted dark blue. To obtain this metallic phase in a 2D plot, we consider  $k_x = 0$  and  $k_x \neq 0$  along each direction ( $\alpha = \{x, y\}$ ), shown by solid and dotted lines, respectively. In pristine  $\beta_{12}$ -borophene, for fermions propagating along the  $x$ -direction, there exist two Dirac fermions at zero energy purely at  $k_y = 0$  and one triplet fermion in the valence band mostly at  $k_y \neq 0$ . Both types of fermions come from the contribution of second and third bands, in agreement with ref. 39 and 40.

The contributions of gas molecule  $\text{NH}_3$  on the electronic states are shown in Fig. 2(b)–(d) along the  $x$ -direction and in Fig. 2(f)–(h) along the  $y$ -direction. Once the molecule is adsorbed on  $\{a, e\}$  atoms, neither Dirac nor triplet fermions exist anymore due to the inversion symmetry breaking. Accordingly, an electronic phase transition from metallic to electron-doped semiconducting takes place, as shown in Fig. 2(b). Interestingly, one extra flat band appears at the same time along the  $y$ -direction in Fig. 2(f) from  $k_x \neq 0$ . If we let the molecule sit on  $\{b, d\}$  atoms, we again expect that the inversion symmetry breaking leads to a significant change in the electronic band structure of  $\beta_{12}$ -borophene. Similarly, Dirac and triplet fermions disappear. Along the  $x$ -direction in Fig. 2(c), we still observe the metallic phase. However, a new flat band is formed in the conduction band. Surprisingly, a new flat band also takes place at the zero Fermi energy along the  $y$ -direction.

For molecule on  $c$  atoms in Fig. 2(c) and (h), however, no significant phenomenon can be observed because the wave functions around the  $c$  atoms cancel each other due to the inversion symmetry and the effect of the molecule is simply washed out. Only a shift/deformation in bands occurs with the presence of the molecule on  $c$  atoms. Thus, in addition to the

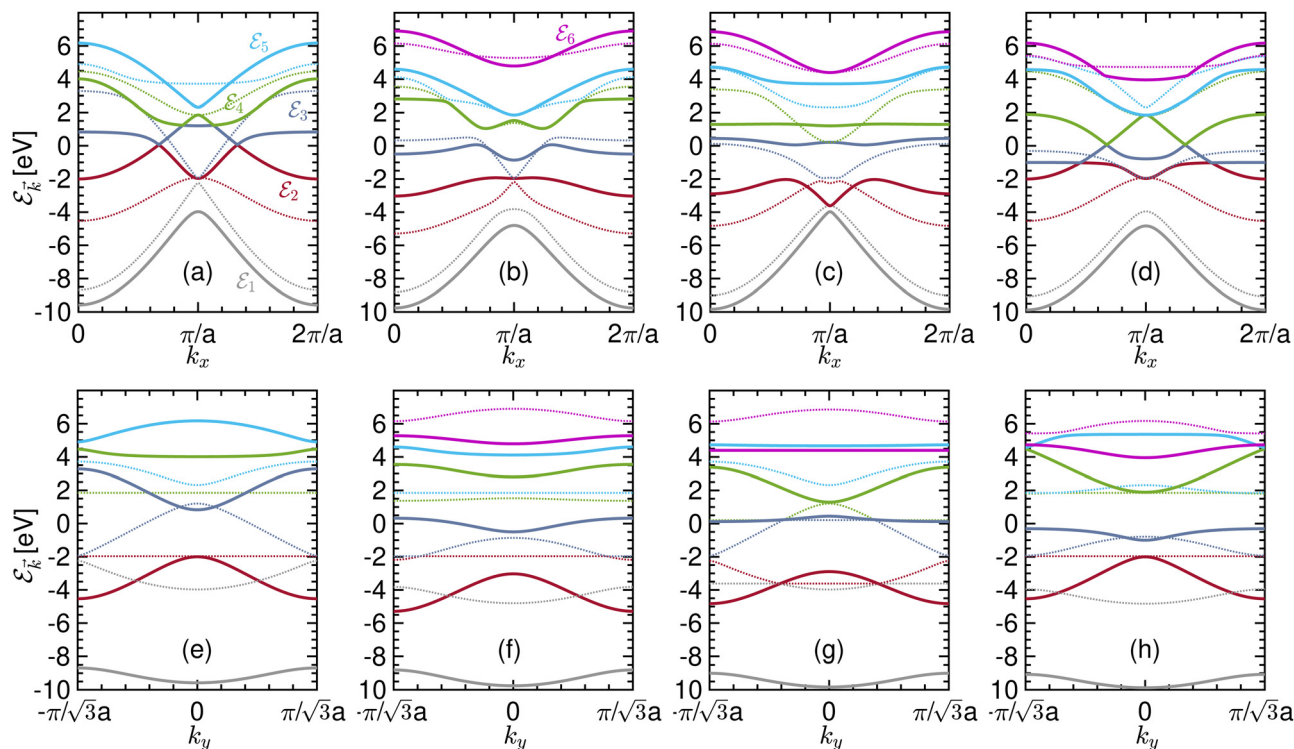


Fig. 2 (a) and (e)) The pristine electronic dispersion of electrons in  $\beta_{12}$ -borophene, which is responsible for the electronic phase along  $x$  and  $y$  directions. To obtain the metallic phase, we consider  $k_x = 0$  and  $k_x \neq 0$  along each direction ( $x = \{x, y\}$ ), shown by solid and dotted lines, respectively. The first and second rows refer to the electronic band structure vs.  $k_x$  and  $k_y$ , respectively, for different configurations of gas adsorption on host atoms. Correspondingly, gas molecule  $\text{NH}_3$  is adsorbed on (b) and (f)) a/e atoms, ((c) and (g)) b/d atoms, and ((d) and (h)) c atoms.

metallic nature of the system which this time occurs between other bands, we still see the Dirac and triplet fermions.

Tuning of bands affects all intrinsic electronic properties of the system. For instance, various filling fractions of the van Hove singularities in the vicinity of the Fermi energy can give rise to exotic phenomena. Microscopically, this can be understood from the overlap of orbitals between the boron atoms in the lattice and gas molecules; the molecule causes structural changes, that displace the electrons. All these features are important for optical responses and they will be discussed in detail in the following.

The light frequency dependence of the optical conductivity shows the characteristic features of a system. It is necessary to point out that in the absence and presence of gas molecules, the optical conductivity is expected to strongly depend on the polarization axis of the incident photon, *i.e.*, in general  $\sigma_{xx} \neq \sigma_{yy} \neq \sigma_{xy/yx}$  holds true. Such anisotropic behavior in the optical spectrum is directly attributed to the electronic property of the system. We hereafter use the indexes ( $d$ ) to label the optical transition between energy bands at  $k_x = 0$  ( $k_x \neq 0$ ).

In the  $x$ -direction, the spectrum consists of five optical peaks and the Drude peak, as shown in the black line in Fig. 3(a), in agreement with ref. 51 and 52. To demonstrate where the peaks come from, we separately show the individual interband transitions in other colors. As can be seen, the Drude peak is formed when the electron excites from  $\epsilon_2^s$  to  $\epsilon_3^s$ , which is that of the Dirac fermion. However, these bands lead to an extra transition

for the peak at  $\hbar\omega \approx 2.55$  eV, which is not contributing much to the total optical response. For the first peak, we purely find the contribution from  $\epsilon_2^d$  to  $\epsilon_3^s$ , which is the strongest response (bright optical peak). For the second peak, the electron excites from  $\epsilon_2^s$  to  $\epsilon_4^s$  with a weaker optical peak compared to the bright one. For the third peak, the transition  $\epsilon_2^s \rightarrow \epsilon_4^d$  is responsible for the response. The fourth peak, which is the weakest response, stems from the transition  $\epsilon_2^s \rightarrow \epsilon_3^d$ . And finally, the last peak mainly originates from the transition  $\epsilon_1^d \rightarrow \epsilon_3^s$ . Such a multi-interband transition is not usual in other 2D materials and it is very important to see how one can tune these transitions for different purposes.

Next, we focus on the impact of gas molecule  $\text{NH}_3$  on the longitudinal optical conductivity of  $\beta_{12}$ -borophene in Fig. 3(b)–(d). We start with molecule-adsorbed {a,e} atoms in Fig. 3(b); total optical response shows three peaks at light energies  $\hbar\omega \approx 0.2$  eV, 3.9 eV, and 4.6 eV. Due to the low-frequency response of the optical conductivity, the system intends to form a redshift spectrum once the sheet is adsorbed with the gas molecule. Our analysis provides two main contributions among multi-interband transitions. The first and third peaks originate from the excitation of electrons from the band  $\epsilon_2^d$  to the band  $\epsilon_3^d$ , corresponding to the non-zero  $k_y$ . While the second peak is formed due to the transition between bands  $\epsilon_2^s$  and  $\epsilon_3^d$ . In contrast to the pristine phase, the lower conduction band and upper valence band do not form a Drude peak once the {a,e} atoms are adsorbed with the molecule.

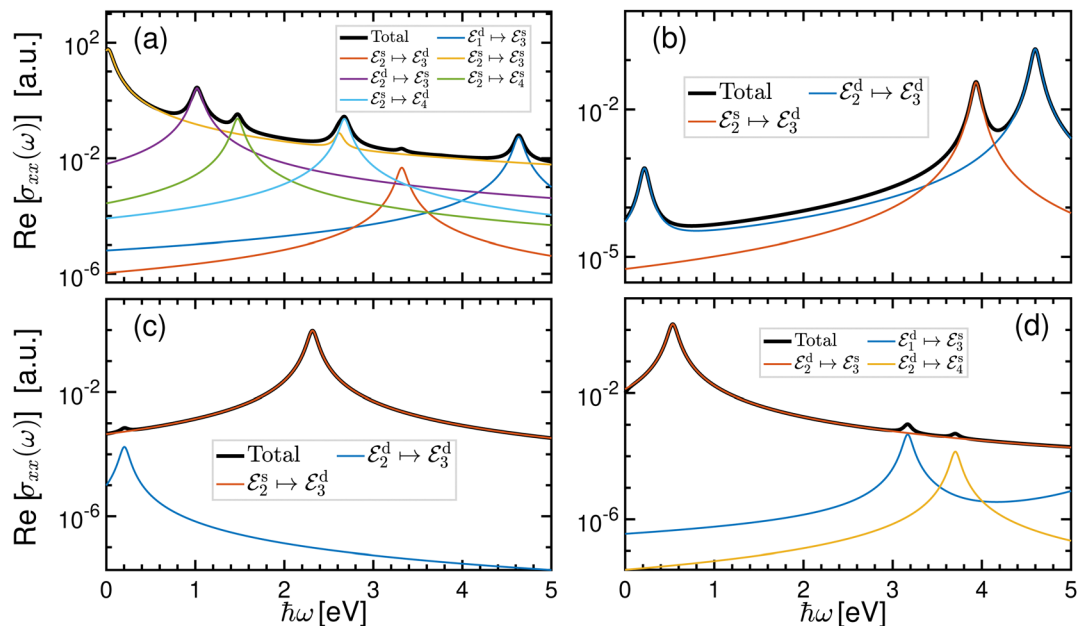


Fig. 3 The frequency dependence of the longitudinal optical conductivity of  $\beta_{12}$ -borophene (a) without and (b)–(d) with changing the position of gas molecule  $\text{NH}_3$  on boron atoms; (b) on {a,e} atoms, (c) on {b,d} atoms, and (d) on {c} atoms.

Upon doping the {b,d} atoms with the gas molecule  $\text{NH}_3$ , the optical spectrum contains only two peaks, one weak peak at low frequency and one strong peak at an intermediate frequency, as shown in Fig. 3(c). The entire response again shows a redshift spectrum. The small peak mainly appears due to  $\varepsilon_2^{\text{d}} \rightarrow \varepsilon_3^{\text{d}}$ , while the strong peak, which is the most significant response in this situation, comes from the interband transition between  $\varepsilon_2^{\text{s}}$  and  $\varepsilon_3^{\text{d}}$ . In Fig. 3(d), we look at the optical response when the gas molecule is adsorbed on c atoms. Since there are three

peaks, there are three possible excitation processes: the excitations from  $\varepsilon_2^{\text{d}}$  to  $\varepsilon_3^{\text{s}}$  for forming the first peak, from  $\varepsilon_1^{\text{d}}$  to  $\varepsilon_3^{\text{s}}$  for forming the second peak, and from  $\varepsilon_2^{\text{d}}$  to  $\varepsilon_4^{\text{s}}$  for forming the third peak. Like two other doping configurations, the system experiences a redshift spectrum when the gas molecule sits on the c atoms.

Turning to the transverse optical conductivity in Fig. 4 under the same conditions, we begin with the pristine  $\beta_{12}$ -borophene in Fig. 4(a). As expected from the inherent anisotropic feature

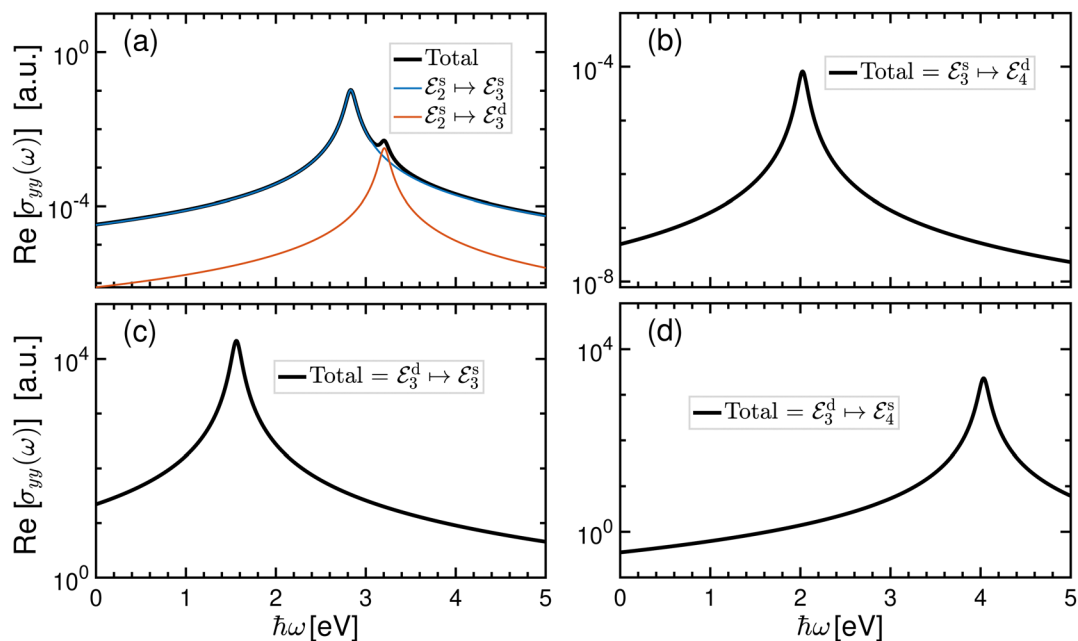


Fig. 4 The same as Fig. 3 but for the transverse optical conductivity.

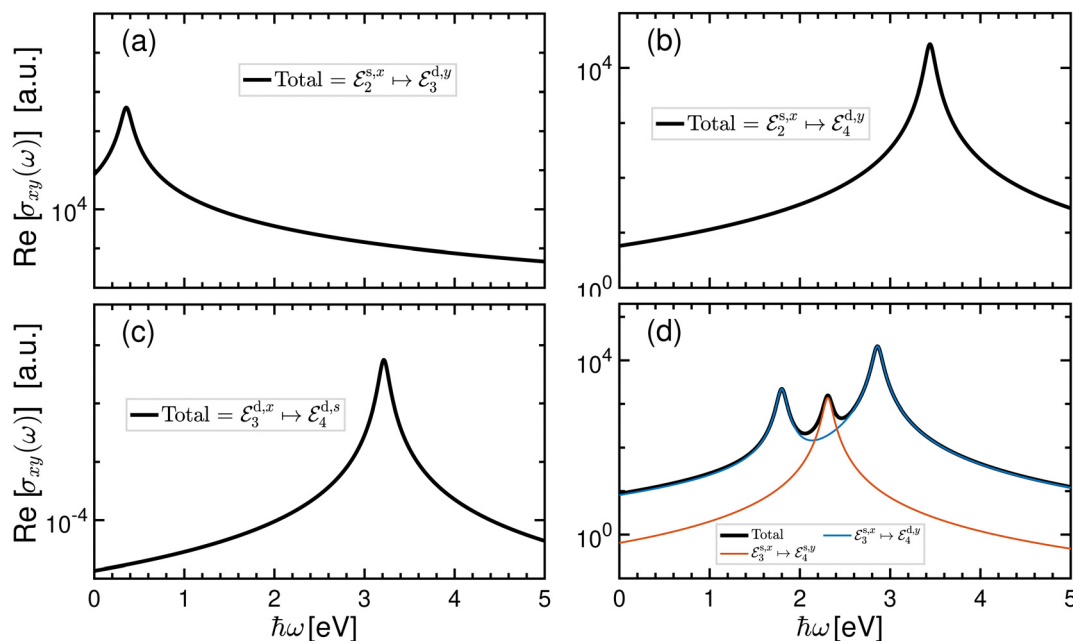


Fig. 5 The same as Fig. 3 but for the Hall optical conductivity.

of the band structure, we observe two optical peaks along the  $y$ -direction, stemming from the excitations  $\varepsilon_2^s \rightarrow \varepsilon_3^s$  and  $\varepsilon_2^s \rightarrow \varepsilon_3^d$ , respectively, for the first and second peak. As soon as the gas molecule  $\text{NH}_3$  is adsorbed on the  $\{a,e\}$  atoms of the sheet, see Fig. 4(b), a single peak forms at  $\hbar\omega \approx 2$  eV, which mainly is formed due to the dominant transition  $\varepsilon_3^s \rightarrow \varepsilon_4^d$ . For molecule on  $\{b,d\}$  atoms, we again observe a single peak at  $\hbar\omega \approx 1.55$  eV from the transitions between bands  $\varepsilon_3^d$  and  $\varepsilon_3^s$ . However, in the case of the molecule on  $c$  atoms, the single peak appears at a higher frequency due to the excitation from the band  $\varepsilon_3^d$  to the band  $\varepsilon_4^s$ . In contrast to the longitudinal component of optical conductivity with a redshift spectrum for all configurations, we find redshift (blueshift) spectrum once the gas molecule is adsorbed on  $\{a,e\}$  and  $\{b,d\}$  (c) atoms.

Finally, we address the impact of adsorbed gas molecule  $\text{NH}_3$  on the Hall optical conductivity of  $\beta_{12}$ -borophene in Fig. 5. In contrast to two other components of the Kubo formula, the Hall component only shows a single peak at low light frequency  $\hbar\omega \approx 0.35$  eV, and the excitation from the band  $\varepsilon_2^s$  along the  $x$ -direction and  $\varepsilon_3^d$  along the  $y$ -direction is responsible for the formed peak, as depicted in Fig. 5(a). If we consider  $\{a,e\}$  atoms in the presence of molecule in Fig. 5(b), we still find a single peak from the band  $\varepsilon_2^s$  along the  $x$ -direction and  $\varepsilon_4^d$  along the  $y$ -direction. In the case of  $\{b,d\}$  atoms in the presence of molecule in Fig. 5(c), however, the single peak originates from the band  $\varepsilon_3^d$  along the  $x$ -direction and  $\varepsilon_4^d$  along the  $y$ -direction. The last configuration is the adsorption of gas molecule on  $c$  atoms in Fig. 5(d). Interestingly, this configuration shows three peaks with two excitation processes: the first process between the band  $\varepsilon_3^s$  along the  $x$ -direction and  $\varepsilon_4^d$  along the  $y$ -direction leads to the first and third peaks, while the process between the band  $\varepsilon_3^s$  along the  $x$ -direction and  $\varepsilon_4^s$  along the  $y$ -direction results in the second peak. Overall, all configurations show a blueshift spectrum for the Hall component.

## 5 Summary

We have analyzed the electronic dispersion and the optical multi-interband transitions for electrons in  $\beta_{12}$ -borophene coupled to adsorbed gas molecules such as  $\text{NH}_3$ ,  $\text{NO}$ ,  $\text{NO}_2$ , and  $\text{CO}$ . We have used the tight-binding model and the Kubo formula, which include contributions from boron atoms, gas molecules, and their coupling, all expressed *via* fully dressed fermionic eigenenergies and eigenstates. We found that depending on the position of the gas molecule on the host boron atoms, various electronic phases and optical transitions appear. Once the gas molecule was located on  $\{a,e\}$  atoms, we found a metallic to the semiconducting phase transition, while the adsorption on  $\{b,d\}$  and  $c$  atoms kept the metallic phase. Consequently, molecules on  $\{a,e\}$  and  $\{b,d\}$  atoms showed a redshift (blueshift) spectrum for longitudinal/transverse (Hall) component of optical conductivity, while molecules on  $c$  atoms led to a redshift (blueshift) optical spectrum for longitudinal (transverse/Hall) component. These findings are important for controlling field-effect transistor-based gas sensors.

## Conflicts of interest

There are no conflicts to declare.

## Acknowledgements

This work was supported by Hue University under the Core Research Program, Grant No. NCM.DHH.2020.01.

## References

- 1 K. S. Novoselov, A. K. Geim, S. V. Morozov, D. Jiang, Y. Zhang, S. V. Dubonos, I. V. Grigorieva and A. A. Firsov, *Science*, 2004, **306**, 666–669.
- 2 A. K. Geim, *Science*, 2009, **324**, 1530–1534.
- 3 C.-C. Liu, H. Jiang and Y. Yao, *Phys. Rev. B: Condens. Matter Mater. Phys.*, 2011, **84**, 195430.
- 4 B. D. Hoi, M. Yarmohammadi and H. A. Kazzaz, *J. Magn. Magn. Mater.*, 2017, **439**, 203–212.
- 5 M. Derivaz, D. Dentel, R. Stephan, M.-C. Hanf, A. Mehdaoui, P. Sonnet and C. Pirri, *Nano Lett.*, 2015, **15**, 2510–2516.
- 6 F.-f Zhu, W.-j Chen, Y. Xu, C.-l Gao, D.-D. Guan, C.-h Liu, D. Qian, S.-C. Zhang and J.-f Jia, *Nat. Mater.*, 2015, **14**, 1020–1025.
- 7 A. Splendiani, L. Sun, Y. Zhang, T. Li, J. Kim, C.-Y. Chim, G. Galli and F. Wang, *Nano Lett.*, 2010, **10**, 1271–1275.
- 8 H. Liu, A. T. Neal, Z. Zhu, Z. Luo, X. Xu, D. Tománek and P. D. Ye, *ACS Nano*, 2014, **8**, 4033–4041.
- 9 H. Bui and M. Yarmohammadi, *J. Magn. Magn. Mater.*, 2018, **465**, 646–650.
- 10 J. Qiao, X. Kong, Z.-X. Hu, F. Yang and W. Ji, *Nat. Commun.*, 2014, **5**, 4475.
- 11 A. Castellanos-Gomez, L. Vicarelli, E. Prada, J. O. Island, K. L. Narasimha-Acharya, S. I. Blanter, D. J. Groenendijk, M. Buscema, G. A. Steele, J. V. Alvarez, H. W. Zandbergen, J. J. Palacios and H. S. J. van der Zant, *2D Materials*, 2014, **1**, 025001.
- 12 C. Özdoğan, S. Mukhopadhyay, W. Hayami, Z. B. Güvenc, R. Pandey and I. Boustani, *J. Phys. Chem. C*, 2010, **114**, 4362–4375.
- 13 I. Boustani, *Surf. Sci.*, 1997, **370**, 355–363.
- 14 M. H. Evans, J. D. Joannopoulos and S. T. Pantelides, *Phys. Rev. B: Condens. Matter Mater. Phys.*, 2005, **72**, 045434.
- 15 H. Tang and S. Ismail-Beigi, *Phys. Rev. Lett.*, 2007, **99**, 115501.
- 16 X. Wu, J. Dai, Y. Zhao, Z. Zhuo, J. Yang and X. C. Zeng, *ACS Nano*, 2012, **6**, 7443–7453.
- 17 E. S. Penev, S. Bhowmick, A. Sadrzadeh and B. I. Yakobson, *Nano Lett.*, 2012, **12**, 2441–2445.
- 18 H. Liu, J. Gao and J. Zhao, *Sci. Rep.*, 2013, **3**, 3238.
- 19 Y. Liu, E. S. Penev and B. I. Yakobson, *Angew. Chem., Int. Ed.*, 2013, **52**, 3156–3159.
- 20 Z. Zhang, Y. Yang, G. Gao and B. I. Yakobson, *Angew. Chem., Int. Ed.*, 2015, **54**, 13022–13026.
- 21 B. Feng, J. Zhang, Q. Zhong, W. Li, S. Li, H. Li, P. Cheng, S. Meng, L. Chen and K. Wu, *Nat. Chem.*, 2016, **8**, 563–568.
- 22 B. Feng, J. Zhang, R.-Y. Liu, T. Iimori, C. Lian, H. Li, L. Chen, K. Wu, S. Meng, F. Komori and I. Matsuda, *Phys. Rev. B*, 2016, **94**, 041408.
- 23 M. D. Stoller, S. Park, Y. Zhu, J. An and R. S. Ruoff, *Nano Lett.*, 2008, **8**, 3498–3502.
- 24 S. Rumyantsev, G. Liu, R. A. Potyrailo, A. A. Balandin and M. S. Shur, *IEEE Sens. J.*, 2013, **13**, 2818–2822.
- 25 E. Akbari, M. Nilashi, A. Alizadeh and Z. Buntat, *Org. Electron.*, 2018, **62**, 181–188.
- 26 L. Kong, A. Enders, T. S. Rahman and P. A. Dowben, *J. Phys.: Condens. Matter*, 2014, **26**, 443001.
- 27 A. T. Lawal, *Talanta*, 2015, **131**, 424–443.
- 28 W. Choi, I. Lahiri, R. Seelaboyina and Y. S. Kang, *Crit. Rev. Solid State Mater. Sci.*, 2010, **35**, 52–71.
- 29 O. Leenaerts, B. Partoens and F. M. Peeters, *Phys. Rev. B: Condens. Matter Mater. Phys.*, 2008, **77**, 125416.
- 30 B. Bhattacharya, U. Sarkar and N. Seriani, *J. Phys. Chem. C*, 2016, **120**, 26579–26587.
- 31 L. Wang, W. Wang, G. Xu, Z. Ji, N. Lu, L. Li and M. Liu, *Appl. Phys. Lett.*, 2016, **108**, 013503.
- 32 V. Shukla, J. Wärnå, N. K. Jena, A. Grigoriev and R. Ahuja, *J. Phys. Chem. C*, 2017, **121**, 26869–26876.
- 33 C.-S. Huang, A. Murat, V. Babar, E. Montes and U. Schwingenschlögl, *J. Phys. Chem. C*, 2018, **122**, 14665–14670.
- 34 C. Hou, G. Tai, Y. Liu and X. Liu, *Nano Res.*, 2022, **15**, 2537–2544.
- 35 F. Opoku and P. P. Govender, *J. Phys. Chem. A*, 2020, **124**, 2288–2300.
- 36 L. Adamska and S. Sharifzadeh, *ACS Omega*, 2017, **2**, 8290–8299.
- 37 A. Mogulkoc, Y. Mogulkoc, D. Kecik and E. Durgun, *Phys. Chem. Chem. Phys.*, 2018, **20**, 21043–21050.
- 38 A. Lherbier, A. R. Botello-Méndez and J.-C. Charlier, *2D Mater.*, 2016, **3**, 045006.
- 39 M. Ezawa, *Phys. Rev. B*, 2017, **96**, 035425.
- 40 B. Feng, O. Sugino, R.-Y. Liu, J. Zhang, R. Yukawa, M. Kawamura, T. Iimori, H. Kim, Y. Hasegawa, H. Li, L. Chen, K. Wu, H. Kumigashira, F. Komori, T.-C. Chiang, S. Meng and I. Matsuda, *Phys. Rev. Lett.*, 2017, **118**, 096401.
- 41 X. Zhang, J. Hu, Y. Cheng, H. Y. Yang, Y. Yao and S. A. Yang, *Nanoscale*, 2016, **8**, 15340–15347.
- 42 P. T. T. Le, T. C. Phong and M. Yarmohammadi, *Phys. Chem. Chem. Phys.*, 2019, **21**, 21790–21797.
- 43 N. Dutta, R. Devi, A. Boruah and S. Acharjee, *Analytic modelling of Quantum Capacitance and Carrier Concentration for  $\beta_{12}$ -Borophene FET based Gas Sensor*, 2023.
- 44 A. H. Pourasl, S. H. S. Ariffin, M. T. Ahmadi, N. Gharaei, R. A. Rashid and R. Ismail, *IEEE Sens. J.*, 2019, **19**, 3726–3732.
- 45 L. T. T. Phuong, T. C. Phong and M. Yarmohammadi, *Sci. Rep.*, 2020, **10**, 9201.
- 46 M. Yarmohammadi and M. R. Ebrahimi, *Phys. Rev. B*, 2019, **100**, 165409.
- 47 M. Yarmohammadi, *AIP Adv.*, 2016, **6**, 085008.
- 48 G. Mahan, *Many-Particle Physics*, Springer, US, 2000.
- 49 T. Stauber, N. M. R. Peres and A. K. Geim, *Phys. Rev. B: Condens. Matter Mater. Phys.*, 2008, **78**, 085432.
- 50 R. d L. Kronig and H. A. Kramers, *Z. Angew. Phys.*, 1928, **48**, 174–179.
- 51 L. T. T. Phuong, B. D. Hoi and M. Yarmohammadi, *Phys. Rev. B*, 2022, **106**, 195409.
- 52 H. V. Ngoc and B. D. Hoi, *J. Phys. D: Appl. Phys.*, 2022, **55**, 395301.